ACS APPLIED MATERIALS & INTERFACES

Research Article

www.acsami.org

Palladium Nanoshell Catalysts Synthesis on Highly Ordered Pyrolytic Graphite for Oxygen Reduction Reaction

Lisandra Arroyo-Ramírez,[†,‡] Diego Rodríguez,[§] Wilfredo Otaño,[‡,§] and Carlos R. Cabrera*[,†,‡]

[†]Department of Chemistry, University of Puerto Rico, San Juan, Puerto Rico 00936-8377

[‡]NASA-URC Center for Advanced Nanoscale Materials, University of Puerto Rico, San Juan, Puerto Rico 00936-8377

[§]Department of Physics-Mathematics, University of Puerto Rico, Cayey, Puerto Rico 00736

Supporting Information

ABSTRACT: A novel approach for the synthesis of palladium (Pd) nanoshells on highly ordered pyrolytic graphite (HOPG) surfaces for the oxygen reduction reaction (ORR) is described. Magnetron sputtering deposition was used to synthesize Pd thin films and nanoshells of different thicknesses on HOPG surfaces. Electrospun polymer fibers mats of poly(ethylene) oxide (PEO) were used as templates for the Pd nanoshells formation. The palladium thicknesses between 25 and 95 nm were deposited by magnetron sputtering. Scanning electron microscopy and energy-dispersive X-ray fluorescence spectroscopy were used to study the morphology and composition of the Pd nanoshells. Electrocatalytic activity toward the ORR and methanol tolerance in oxygen saturated 0.5 M H_2SO_4 solution was determined. Palladium nanoshells presented higher electrocatalytic activity toward ORR than Pd thin films of similar electrodes thicknesses and geometric area. Since palladium has higher methanol tolerance than platinum, the Pd nanoshells are promising electrode materials for direct methanol fuel cells (DMFC).

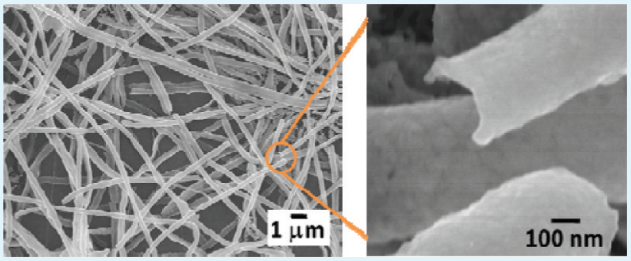

KEYWORDS: *sputtering deposition, electrospinning, Pd, catalysis, oxygen reduction reaction, methanol tolerant, direct methanol fuel cells*

INTRODUCTION

Polymer electrolyte membrane fuel cells (PEMFC) promise to be the future energy technology for transportation and portable devices. In fuel cells, one of the most challenging areas is to find nonplatinum catalysts for oxygen reduction reaction (ORR) that allow high efficiency and durability.[1,2] Direct methanol fuel cells (DMFC) cathodes have the problem of requiring high cost catalysts and their degradation due to methanol cross-over.[3,4] Moreover, the deposition methods for the catalysts are complex and time-consuming. To solve this drawback, it is necessary to find a catalyst with high methanol tolerance and simple methodology for its deposition. For these reasons, oxygen reduction reaction catalyst is a key challenge for the fuel cell technology commercialization. It is known that palladium and Pd-based alloys have resulted in extremely active catalysts for the oxygen reduction reaction (ORR).[5−7] Moreover, Pd is a good catalyst for the ORR in DMFC cathode because it has a high tolerance toward methanol.[8,9]

Sputtering is a technique that allows easy modification of different substrates with a great variety of materials and high degree of control of their properties.[10] Sputtering is a physical process that ejects surface atoms from a target due to the ions bombarding the surface. DC plasma is used for sputter deposition of metallic and semiconductors materials. This requires a negative charged target and a grounded surface. "This process has been a manufacturing technology for over 120 years".[10] Through the years, sputtering deposition has been used for the synthesis of materials for sensors,[11,12] solar cells,[13−15] fuel cells,[16−19] and biological[20,21] applications, among others. In the literature, the use of sputtered catalysts layer on Nafion membrane reducing the methanol crossover from the anode to the cathode in the DMFC has been reported.[22,23] Also, using the sputtering technique allows reduction on the electrodes catalysts loading in PEM fuel cells.[18,24−26]

Electrospinning is a simple process to produce fibers from polymer solutions due to electrostatic forces.[27] The electrospun polymer fibers can be obtained with average diameters ranging from a few nanometers to micrometers depending on the content of polymer solution and electrospinning parameters.[28,29] Several studies have been done on the use of electrospun polymer fiber for the formation of catalysts for PEM fuel cells.[29,30] Recently, W. Zhang reported high power density in a hydrogen/air fuel cell using electrospun nanofibers electrode.[31] Sputtering allows the metal deposition on top of polymer fibers to produce nanostructures.

The present research focus is on the use of a simple method for the synthesis of palladium nanocatalysts on highly ordered

Received: December 30, 2011
Accepted: February 23, 2012
Published: February 23, 2012

pyrolytic graphite (HOPG) surfaces for oxygen reduction reaction (ORR), as a model to be used for fuel cell applications. In this work, the study of palladium catalytic nanostructures (thin films and nanoshells) synthesized using sputtering and electrospinning techniques and their electrochemical characterization is presented. This method is an alternative to reduce electrode preparation time for fuel cells as compared to the conventional method (paste method) as well as to enhance the catalytic activity. The Pd nanostructures were characterized by cyclic and linear sweep voltammetry and scanning electron microscopy with energy-dispersive X-ray fluorescence spectroscopy (SEM/EDS). The palladium nanoshells catalysts present higher activity for the oxygen reduction reaction than palladium thin films. Moreover, the palladium nanostructures present higher methanol tolerance than platinum catalysts.

EXPERIMENTAL SECTION

Synthesis of Palladium Thin Films. An exfoliated piece of highly ordered pyrolytic graphite (HOPG) spi-2 grade was used as a carbon support for the thin films. A 99.999% pure palladium (Pd) target (Kurt J. Lesker) was used to deposit the Pd thin films by sputtering technique. The sputtering chamber had a vacuum pressure below 5×10^{-6} Torr. Briefly, palladium deposition on HOPG surface was carried out by direct current magnetron sputtering at deposition pressures of 13 mTorr, 50 W of power, and ultrahigh purity argon atmosphere.[32] Palladium was deposited at different time periods, and the film thicknesses were measured by profilometry. A calibration curve of thickness as a function of sputtering time was used to deposit films with four different thicknesses: 25, 50, 75, and 95 nm of palladium.

Synthesis of Palladium Nanoshells. (a) Electrospun poly(ethylene) oxide (PEO) fibers on the highly ordered pyrolytic graphite (HOPG) surfaces were used as templates for the nanoshells formation.[33] These polymer fiber mats were deposited by electrospinning technique. The polymer solution of 0.056 g of PEO (average M_v ~900 000; Sigma-Aldrich), 1.6 mL of ethanol (Sigma-Aldrich), and 0.4 mL of deionized water was stirred for 3 h before the polymer fiber mat preparation. PEO fibers were deposited on HOPG surface (collector) by pumping the solution at 0.50 mL/h through a syringe, with an applied potential of 19 kV, and a distance from syringe tip to collector of 28 cm. (b) Palladium was deposited by sputtering on top of the electrospun fibers mat as described above. (c) Then, the palladium modified fiber mats were heated at 320 °C for 2 h under Ar atmosphere to remove the fiber cores and obtain the Pd nanoshells. From the deposition times used, it is calculated that the palladium nanoshells film thicknesses were between 25 and 95 nm at the center decreasing toward the edges (in a crescent moon shape).[34] Figure 1S in the Supporting Information presents a diagram showing the synthesis process of the Pd nanoshells.

Physical Characterization. Field emission scanning electron microscopy (FE-SEM) with energy-dispersive X-ray fluorescence spectroscopy (EDS) (JEOL JSM-7500F) and SEM/EDS (JEOL-5800LV) were used for the morphological and composition characterization. Images and EDS spectra were taken using an accelerating voltage of 15 and 30 keV, respectively.

Electrochemical Characterization. The electrochemical measurements were performed using a potentiostat AutoLab (PGSTAT 30). A three-electrode cell was employed in all experiments with a Pt spiral auxiliary electrode, mercury-mercurous sulfate ($Hg|Hg_2SO_4$; K_2SO_4, sat.; 0.64 V vs NHE)[35] as reference electrode, and HOPG modified with the Pd sputtered nanostructure as working electrode. The cyclic voltammetry (CV) was carried out in a potential window between −0.65 and 0.9 V vs $Hg|Hg_2SO_4$ in 0.5 M H_2SO_4 at a scan rate of 100 mV s^{-1}. Linear sweep voltammetry (LSV) was done at potentials between 0.6 and −0.5 V vs $Hg|Hg_2SO_4$ in oxygen saturated 0.5 M H_2SO_4 solution for 15 min at a scan rate of 5 mV s^{-1}. The study of the palladium nanocatalysts tolerance toward methanol was done in 1.0 M MeOH in 0.5 M H_2SO_4 solution saturated with oxygen at a scan rate of 5 mV s^{-1}. The geometrical areas for the Pd nanostructures and the platinum (Pt) film electrodes (Maxtek) were 0.145 and 1.131 cm^2, respectively. The electroactive surface area (ESA) was determined by measuring the charge of the Pd oxide reduction region, from the cyclic voltammetry in 0.5 M H_2SO_4, divided by the theoretical charge for a palladium oxide monolayer reduction (424 μC cm^{-2}).[36,37] The roughness factor of the films was calculated using the electroactive surface area divided by the geometrical area.[38] The deionized water used for the experiments was previously distilled and pumped through a Nanopure system (Barnstead) to give 18 MΩ-cm resistivity. All electrochemical experiments were carried out at room temperature.

RESULTS AND DISCUSSION

Palladium sputter deposition on highly ordered pyrolytic graphite (HOPG) surfaces with different thicknesses was carried out to determine their surface and electrochemical properties for the oxygen reduction reaction (ORR) without and with methanol. Synthesis by sputtering deposition of the palladium thin films on HOPG surfaces showed homogeneous and smooth surface.[33] FE-SEM was used to obtain more surface morphology information about the Pd depositions on HOPG surface. Figure 1 shows high resolution SEM images of the sputtered Pd thin films on HOPG surfaces with thickness between 25 and 95 nm. The images clearly show very uniform distribution of the sputtered Pd electrocatalysts. We can observe that Pd films are formed with average nanoparticles diameter size between 12 and 23 nm (see Table 1). L. Gu et al. have produced gold (Au) nanoparticles with average size of 10 nm using the sputtering method, although no deposited

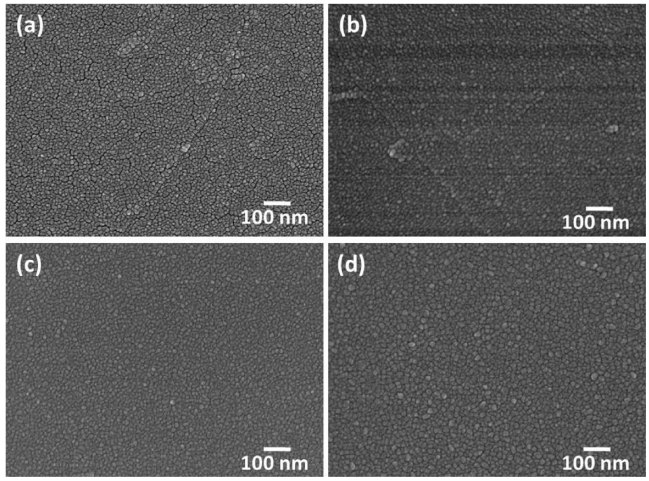

Figure 1. Field emission scanning electron microscopy (FE-SEM) images for (a) 25 nm, (b) 50 nm, (c) 75 nm, and (d) 95 nm Pd thin films on HOPG surfaces deposited by dc-magnetron sputtering at 13 mTorr.

Table 1. Morphological Dimensions of the Pd Thin Films and Pd Nanoshell Structures[a]

Pd thickness (nm)	thin films particles size (nm)	nanoshells diameter size (μm)
25	12.3 ± 5.1	0.37 ± 0.10
50	15.0 ± 5.6	0.60 ± 0.23
75	17.6 ± 4.4	0.62 ± 0.19
95	23.3 ± 6.2	0.45 ± 0.12

[a]Note: Pd thickness for the nanoshells refers to the maximum thickness at the center of the nanoshell as shown in Figure 1Sd, Supporting Information.

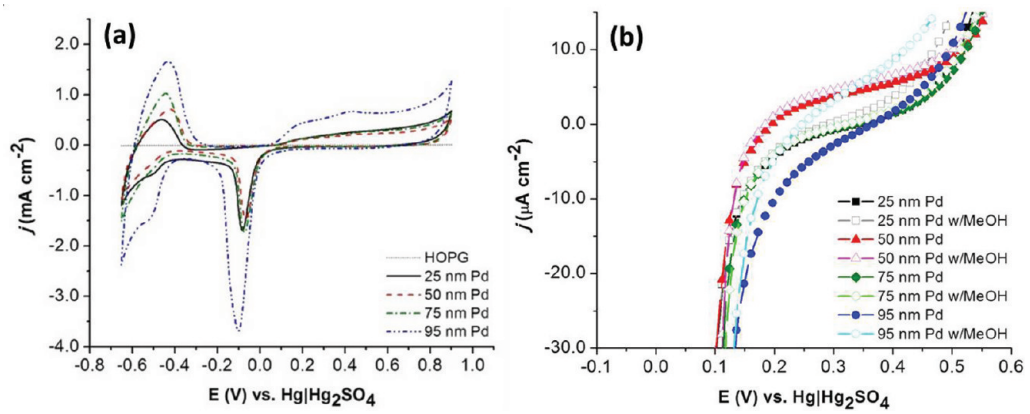

Figure 2. (a) Cyclic voltammograms for the 25, 50, 75, and 95 nm Pd thin films on HOPG surfaces and (b) linear sweep voltammetry without (solid symbol) and with 1.0 M MeOH (open symbol) in 0.5 M H_2SO_4 purged with oxygen for 15 min before each experiment.

Table 2. Cathodic Current Densities for the Oxygen Reduction Reaction at 0.100 V vs. $Hg|Hg_2SO_4$ in 0.5 M H_2SO_4, Electrochemical Charge of the Palladium Surface Oxide Reduction, and Calculated Surface Area for the Pd Nanostructures with Different Thicknesses

Pd nanostructures	Pd thickness (nm)	current density (A/cm^2) at 0.100 V[a]	electrochemical charge (μC)[b]	palladium surface area (cm^2)[c]	roughness factor
thin film	25	-3.23×10^{-5}	197	0.465	3.20
	50	-3.19×10^{-5}	177	0.417	2.88
	75	-5.68×10^{-5}	207	0.489	3.37
	95	-1.06×10^{-4}	565	1.332	9.19
nanoshells	25	-6.90×10^{-5}	284	0.669	4.61
	50	-1.49×10^{-4}	803	1.894	13.1
	75	-7.17×10^{-5}	415	0.978	6.74
	95	-2.97×10^{-4}	950	2.240	15.4

[a]Cathodic current densities for oxygen reduction reaction at 0.100 V vs $Hg|Hg_2SO_4$. The solution was purged with oxygen for 15 min before each experiment. Geometrical area is 0.145 cm^2. [b]Electrochemical charge of the palladium surface oxide reduction. [c]Palladium surface areas calculated from the electrochemical palladium surface oxide reduction charge and the conversion factor of 424 μC cm^{-2}.[37]

thickness was reported.[16] On the other hand, I. Radev reported mean sizes from 250 to 50 nm for sputtered Pt thin films with thickness between 150 and 1000 nm.[17]

Our 25 and 50 nm Pd thin films presented small cracks that create discontinuous films; the 50 nm film showed smaller crack amounts as shown in Figure 1a,b. A crack-free thin film, for Pd thickness of 75 and 95 nm, is presented in Figure 1c,d. Z. Q. Ma and co-workers reported cracks and crack-free areas in 1 μm Pt/Pd–Ag/Pt sputtered film over Nafion membrane.[22] S. R. Yoon et al. reported many cracks in 100 nm Pd film on Nafion membrane.[23] Also, R. O'Hayre et al. reported as low as 5 nm Pt film on Nafion membrane presenting isolated cracks across the surface.[26] They explained that these cracks occurred due to dehydration and rehydration of the Nafion membranes during and after the sputtering process. According to our results, we could deposit Pd thin films on a gas diffusion layer (GDL) and should obtain a more uniform and crack-free catalyst than obtained on Nafion membranes.

Cyclic voltammograms for the HOPG surface (short dash line) and 25 nm (straight line), 50 nm (dash line), 75 nm (dash dot line), and 95 nm (dash dot dot line) Pd thin films in 0.5 M H_2SO_4 solution at scan rate of 100 mV/s are presented in Figure 2a. In the cyclic voltammetry, it is observed that the Pd oxide reduction peaks for 25 and 75 nm Pd thin film have similar current densities. While, for the hydrogen adsorption/desorption peaks, the 75 nm Pd thin film showed higher current densities (see Figure 2a). The 50 nm Pd thin film has lower current in the Pd oxide reduction than the 25 nm Pd thin film but higher hydrogen desorption. The 95 nm Pd thin film has the highest current density for Pd oxide reduction and hydrogen adsorption/desorption peaks. The 25 nm Pd thin film was expected to have the higher electroactive surface area due to the smaller particle size. As shown in Figure 1a, the sample has regions with cracks that can create a discontinuous film and reduce the electroactive surface area. Table 2 summarizes the electrochemical results for the thin films and nanoshells with different Pd thickness. The 95 nm Pd thin film has the electroactive surface area (ESA) and roughness factor of 1.33 cm^2 and 9.19, respectively.

Figure 2b shows the linear sweep voltammograms (LSV) for the 25 nm (square symbol), 50 nm (triangle symbol), 75 nm (diamond symbol), and 95 nm (circle symbol) Pd thin films on HOPG surfaces in 0.5 M H_2SO_4 and 1.0 M MeOH/0.5 M H_2SO_4 solution saturated with oxygen at scan rate of 5 mV/s. From LSV, similar ORR electrocatalytic activity for the Pd thin films is observed. The 95 nm Pd thin film has the highest positive shift in the ORR onset potential at 0.100 V. The thicknesses of the sputtered palladium thin films have little effect in the catalytic activity toward oxygen reduction with only a few mV of difference in the onset potential between the 25 and 75 nm of Pd (see Table 3), but between the 25 and 95 nm of Pd thin films, there is a difference of approximately 38 mV on the ORR onset potential. The 95 nm Pd thin film showed higher ORR electrocatalytic activity than the other thin films. The sputtered Pd thin films have similar electrocatalytic activity when we compare the ORR with and without MeOH, demonstrating high methanol tolerance.

Table 3. Oxygen Reduction Reaction Onset Potentials at −0.20 μA cm^{-2} for Pd Thin Films and Pd Shells Nanostructures without and with Methanol[a]

	thin films		nanoshells	
Pd thickness (nm)	E (V)	E (V) w/MeOH	E (V)	E (V) w/MeOH
25	0.114	0.114	0.125	0.117
50	0.113	0.117	0.161	0.164
75	0.123	0.126	0.154	0.161
95	0.152	0.144	0.196	0.207

[a]Note: All potentials vs. Hg|Hg_2SO_4.

Electrospinning technique was used to deposit the polyethylene oxide (PEO) polymer fibers mats on HOPG surfaces as template to form Pd nanoshells. These polymer fibers were coated with Pd using the sputtering technique. After Pd sputter deposition, the samples were heated in an inert argon atmosphere to remove the polymer core and obtain the Pd nanoshells (see Figure 1S in the Supporting Information). Previously, we reported that increasing the amount of PEO fiber mats (from nondense to a dense mat) while keeping the same palladium thickness achieved the best ORR catalytic activity.[33] Therefore, for this work, electrospun dense PEO polymer fiber mats on the HOPG surfaces was done. Figure 3

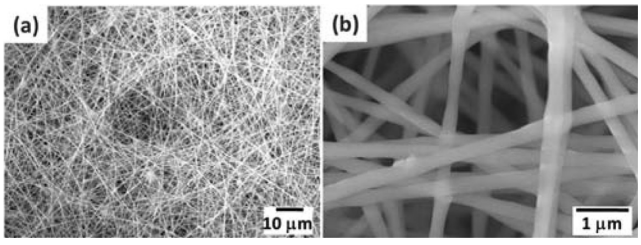

Figure 3. Field emission scanning electron microscopy (FE-SEM) images of electrospun poly(ethylene) oxide (PEO) polymer fibers on HOPG surfaces at (a) 1000× and (b) 20 000× magnification.

shows the SEM images of the electrospun PEO fiber mats on the HOPG surfaces. These polymer fibers form a very uniform network and only few bead-on-fibers may be found as shown in Figure 3b. The HOPG surface is completely covered with the PEO fibers mat. The polymer fibers have a diameter range between 0.29 and 0.65 μm with an average value of (0.41 ± 0.10) μm. This in agreement with W. K. Son et al., which reported electrospun PEO fibers with diameters from 0.36 to 1.96 μm with different polymer solution content and electrospinning parameters.[39]

The synthesis of the palladium nanoshells was carried out by the modification of the HOPG surface by adding the PEO polymer fibers mat, followed by sputtering Pd on top of them and heating to remove the PEO polymer core. The sputtering times used to coat the PEO fiber mats with Pd were the same ones used to prepare films between 25 and 95 nm. Figure 4 shows Pd sputtered on PEO fiber mats after heat treatment in argon to 320 °C. In these SEM images, we observe (a) 25 nm, (b) 50 nm, (c) 75 nm, and (d) 95 nm Pd nanoshells on HOPG surfaces. Table 1 summarizes the average diameter of the nanoshells with different Pd thickness. The Pd nanoshells have average diameters between 0.37 and 0.62 μm. The Pd nanoshells average diameter increases with increasing the palladium thickness except for the 95 nm Pd shell. The 95 nm Pd nanoshells have smaller average diameter maybe because the

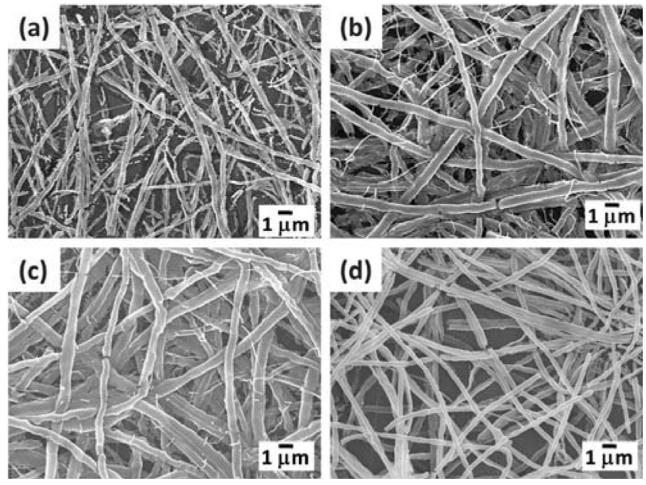

Figure 4. Field emission scanning electron microscopy (FE-SEM) images for (a) 25 nm, (b) 50 nm, (c) 75 nm, and (d) 95 nm Pd nanoshells on HOPG surfaces at 5000× magnification.

shells, with a u-type shape, are more closed than the 50 and 75 nm Pd nanoshells. This result confirms the increase in the diameter sizes of the nanostructures after sputter Pd on the polymer fibers. Pantojas and co-workers explained in detail the shell formation by mathematical simulations.[34] Also, they demonstrated the different nanoscale structures formation with the variation in the electrospinning and sputtering parameters.

Figure 5a show images for the 95 nm Pd nanoshells, and Figure 5b is a zoom that shows the half tube nanostructure.

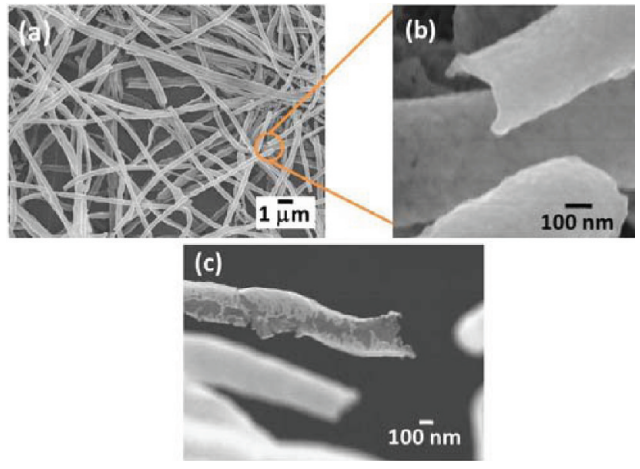

Figure 5. Field emission scanning electron microscopy (FE-SEM) images for 95 nm Pd nanoshells deposited on HOPG surfaces showing the shell like structure at (a) 5000×, (b) 100 000×, and (c) 50 000× magnification.

These images show the shell-like structures resulting after elimination of the PEO fiber (see Figure 5b,c). The Pd shells have a rougher surface when compared with the polymer fibers (see Figures 5c and 3b). An EDS spectrum was used to determine the nanoshells composition. Figure 6 shows the EDS spectrum for the 25 nm Pd nanoshells and its corresponding SEM image. The EDS spectrum shows the presence of palladium, carbon (support), and oxygen. The sputtering in combination with the electrospinning techniques does not introduce impurities into the electrocatalytic nanostructures. Figure 7 shows the SEM image and map lines scan of 75 nm Pd

dx.doi.org/10.1021/am201860r | ACS Appl. Mater. Interfaces 2012, 4, 2018−2024

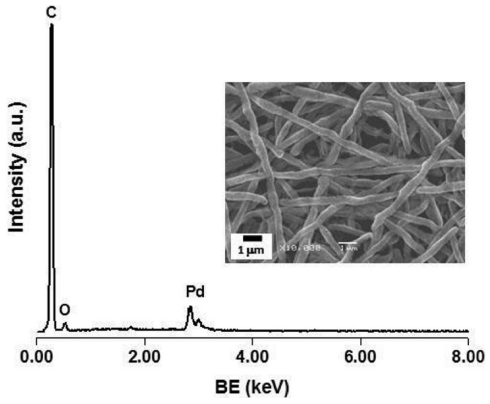

Figure 6. Energy-dispersive X-ray fluorescence spectroscopy (EDS) spectrum for 25 nm Pd nanoshells on HOPG surfaces. Inset: Scanning electron microscopy (SEM) image at 10 000× magnification.

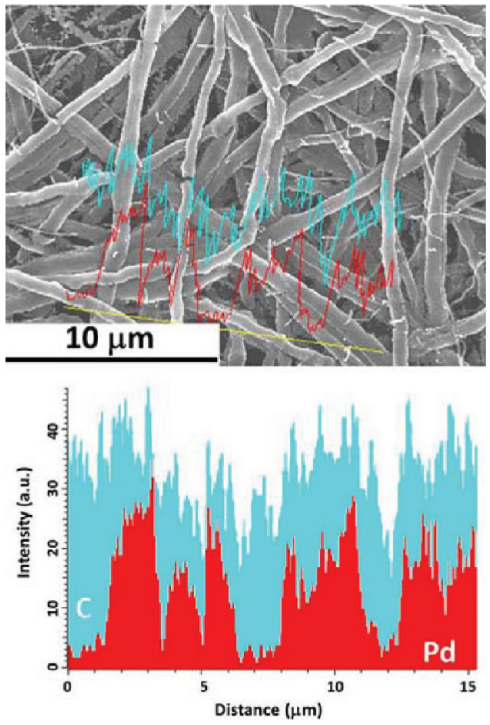

Figure 7. Field emission scanning electron microscopy (FE-SEM) image at 5000× magnification and energy-dispersive X-ray fluorescence spectroscopy (EDS) map lines for carbon and palladium of 75 nm Pd nanoshells on HOPG surfaces.

nanoshells. Clearly, the maps line scan showed that the nanoshells are of palladium. Also, we can observe the map lines scan corresponding to the support (carbon). The combination of these techniques allows the nanocatalysts synthesis and deposition directly on gas diffusion layers (GDL) reducing preparation time of the membrane electrode assembly (MEA) for polymer electrolyte membrane fuel cells (PEMFC). To our knowledge, this is the first time electrospinning and sputtering techniques were used in this tandem configuration for fuel cell applications.

Figure 8a shows cyclic voltammograms for HOPG (short dash line), PEO fiber mats on HOPG [PEO/HOPG] (dash line), and 25 nm Pd nanoshells on HOPG (straight line). The HOPG surface and polymer fibers on HOPG have similar electrochemical behavior. Meanwhile, the 25 nm Pd shell nanostructures show the typical electrochemical behavior of palladium. The HOPG surface is shiny gray, and after being electrospun, the polymer fibers mat changes to grayish white. The Pd nanoshells are gray. After electrochemical characterization, HOPG and Pd nanoshells remain with the same color. However, the PEO/HOPG changed to a shiny gray similar to the HOPG due to the polymer dissolution in aqueous solution. Figure 8b shows ORR activity (straight line) and methanol tolerance (dash line) for PEO fiber mats and 25 nm Pd nanoshells on HOPG. The PEO/HOPG does not have electrocatalytic activity while 25 nm Pd shells have ORR activity and high methanol tolerance.

Figure 9a show cyclic voltammograms for the HOPG surface (short dash line) and 25 nm (straight line), 50 nm (dash line), 75 nm (dash dot line), and 95 nm (dash dot dot line) Pd nanoshells in 0.5 M H_2SO_4 solution at scan rate of 100 mV/s. In the cyclic voltammograms, it was observed that the Pd oxide reduction peaks for 25 and 75 nm Pd nanoshells have similar current densities. However, the hydrogen absorption/desorption peaks for 75 nm Pd showed higher current. The 50 nm Pd nanoshells showed lower currents in the Pd oxide reduction than 95 nm Pd nanoshells but higher current than 25 and 75 nm Pd nanoshells. The 95 nm Pd nanoshells and 75 nm Pd nanoshells have the highest current for Pd oxide reduction and adsorption/desorption hydrogen peaks, respectively. The values of ESA and roughness factor for the nanoshells are much higher than those of the thin film with the same Pd thickness (see Table 2). The 95 nm Pd nanoshells have the higher electroactive surface (ESA) area and roughness factor of 2.24 cm^2 and 15.4, respectively.

Figure 9b shows the ORR activity for the 25 nm (square symbol), 50 nm (triangle symbol), 75 nm (diamond symbol), and 95 nm (circle symbol) Pd nanoshells on HOPG surfaces without (solid symbol) and with methanol (open symbol) solutions saturated with oxygen at 5 mV/s. The 50 and 75 nm Pd nanoshells have similar ORR catalytic activity. The 50 and 75 nm Pd nanoshells have only a few mV of difference in the ORR onset potential (see Table 3). On the other hand, for the Pd nanoshells between 25 and 95 nm, there is a difference of approximately 71 mV at current density of −20 $\mu A/cm^2$. The 95 nm Pd nanoshells have the highest ORR electrocatalytic activity with a current density of -2.97×10^{-4} A at 0.1 V vs Hg| Hg_2SO_4. Oxygen reduction reaction activities are, from best to worst for the Pd nanoshells: 95 nm ≫50 nm ≥75 nm ≫25 nm. The ORR activity with methanol of some of these catalysts has a slightly positive potential shift of a few mV (see Table 3). The Pd shell nanostructures have similar ORR electrocatalytic activity without and with MeOH, demonstrating high methanol tolerance. A study of these sputtered palladium electrocatalytic nanostructures on carbon cloth for the DMFC cathode is underway.

Figure 10 shows the oxygen reduction electrocatalytic activity without (straight line) and with (dash line) methanol for platinum (Pt), 95 nm Pd thin films, and 95 nm Pd shell nanostructures. Pt film electrode has a positive onset potential shift of approximately 75 mV when compared with the Pd nanoshells (see Figure 3S in the Supporting Information). The Pt electrode has higher ORR activity but the lowest methanol tolerance (see Figure 10a). On the other hand, the 95 nm Pd thin films and 95 nm nanoshells have high ORR catalytic activity and the highest methanol tolerance. Table 3 presents the potential for the ORR for the Pd thin films and Pd shells nanostructures at current density of −20 $\mu A/cm^2$. The Pd

dx.doi.org/10.1021/am201860r | ACS Appl. Mater. Interfaces 2012, 4, 2018−2024

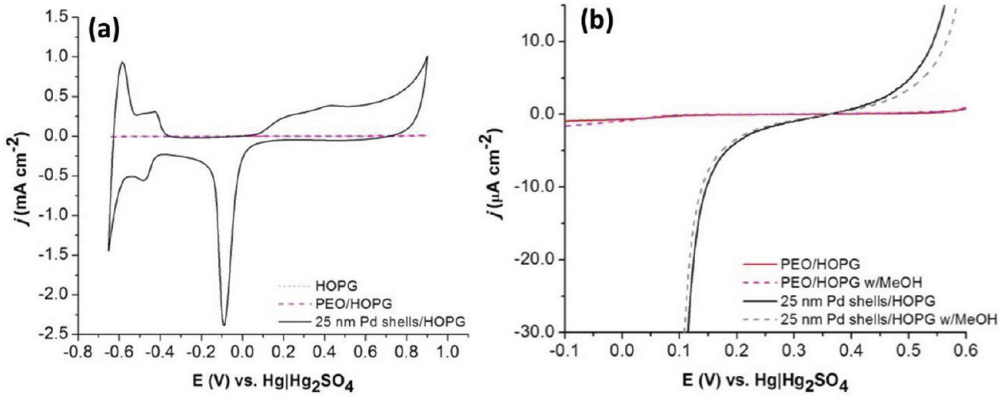

Figure 8. (a) Cyclic voltammograms of bare and PEO fibers and 25 nm Pd nanoshells surface modified HOPG in 0.5 M H_2SO_4 and (b) linear sweep voltammetry without (straight line) and with 1 M MeOH (dash line) in 0.5 M H_2SO_4 purged with oxygen for 15 min before each experiment.

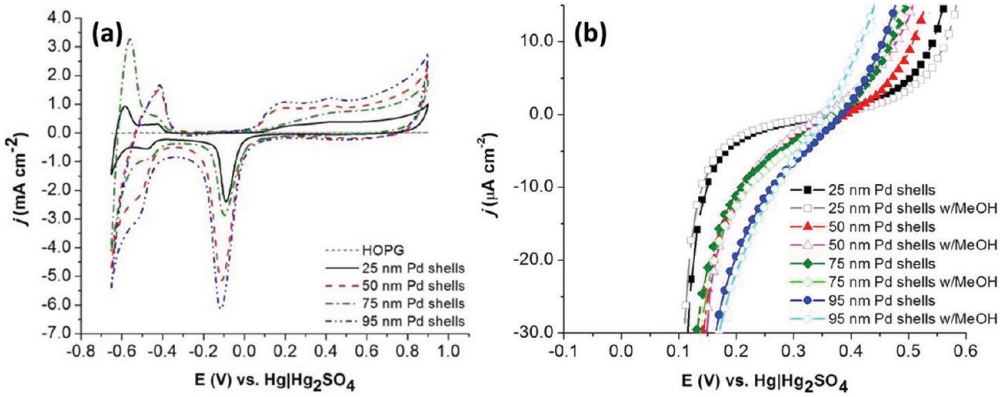

Figure 9. (a) Cyclic voltammograms for the 25, 50, 75, and 95 nm Pd nanoshells on HOPG surfaces in 0.5 M H_2SO_4 and (b) linear sweep voltammetry without (solid symbol) and with 1 M MeOH (open symbol) in 0.5 M H_2SO_4 purged with oxygen for 15 min before each experiment.

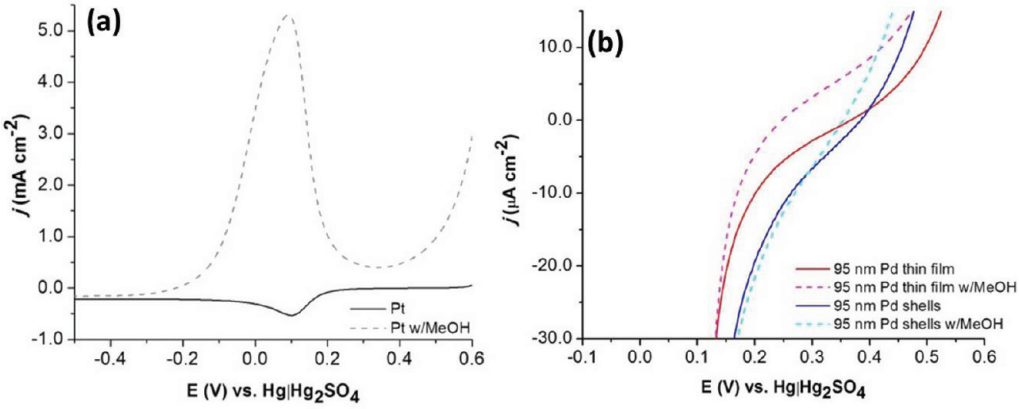

Figure 10. Oxygen reduction reaction activity (straight line) and methanol tolerance (dash line) for (a) Pt film electrode (Maxtek) and (b) 95 nm Pd thin film and nanoshells on HOPG surfaces.

nanoshells have better ORR activity than the Pd thin films. The 95 nm Pd nanoshells have a positive potential shift of approximately 82 mV when compare with the 25 nm Pd thin film. The Pd thin films have lower ORR activity due to the fact that the uppermost surface is the only one that carries out the catalysis. The formation of the shell-like nanostructures increases the electroactive surface area compared with a thin film. The shell nanostructures improve that ORR catalytic activity because the top and bottom of the Pd nanoshells are able to carry out the catalysis. This research will be essential in the formation of nanostructured electrocatalysts for the cathodes in direct methanol fuel cell (DMFC).

CONCLUSIONS

The palladium catalytic nanostructures have been successfully synthesized using the magnetron sputtering and electrospinning techniques. SEM images for sputtered Pd on HOPG surfaces show thin films formed by nanoparticles with average diameters below 25 nm independent of the amount of Pd deposited. The electrospun PEO fiber mats on HOPG surfaces allow the synthesis of the Pd nanoshells by sputtering

dx.doi.org/10.1021/am201860r | ACS Appl. Mater. Interfaces 2012, 4, 2018–2024

deposition. The palladium nanocatalysts have activity for the ORR and high methanol tolerance. The Pd nanoshells have better ORR activity than Pd thin films. The present investigation confirms that shell nanostructures improve the ORR catalytic activity compared with Pd thin film due to the increase on the surface area. The results suggest that using the sputtering and electrospinning techniques in a tandem configuration can be used as a simple method for the synthesis of catalysts for the cathode of direct methanol fuel cells.

■ ASSOCIATED CONTENT

Supporting Information

A diagram of the Pd nanoshells synthesis, SEM images of the HOPG surface and ORR activity of the Pt film and the 95 nm Pd thin film and nanoshells on HOPG. This information is available free of charge via the Internet at http://pubs.acs.org.

■ AUTHOR INFORMATION

Corresponding Author

*E-mail: carlos.cabrera2@upr.edu.

Notes

The authors declare no competing financial interest.

■ ACKNOWLEDGMENTS

This research was supported in part by NASA-URC Grant No. NNX10AQ17A and NASA Training Grant No. NNG056678H (PR Space Grant). DRV work was supported by Department of Energy Grant DE-FG02-08ER46526. The authors acknowledge the use of the IFN Nanoscopy Facility (NSF-EPSCoR Institute for Functional Nanomaterials Grant No. OIA-0701525 and EPS-1002410) and Material Characterization Center (MCC) at UPR-RP.

■ REFERENCES

(1) Gewirth, A. A.; Thorum, M. S. *Inorg. Chem.* **2010**, *49*, 3557.
(2) Wang, B. *J. Power Sources* **2005**, *152*, 1.
(3) Prabhuram, J.; Zhao, T. S.; Liang, Z. X.; Yang, H.; Wong, C. W. *J. Electrochem. Soc.* **2005**, *152*, A1390.
(4) Bezerra, C. W.B.; Zhang, L.; Liu, H.; Lee, K.; Marques, A. L.B.; Marques, E. P.; Wang, H.; Zhang, J. *J. Power Sources* **2007**, *173*, 891.
(5) Shao, M. H.; Huang, T.; Liu, P.; Zhang, J. K.; Sasaki, K.; Vukmirovic, M. B.; Adzic, R. R. *Langmuir* **2006**, *22*, 10409.
(6) Antolini, E. *Energy Environ. Sci.* **2009**, *2*, 915.
(7) Shao, M.-H.; Sasaki, K.; Adzic, R. R. *J. Am. Chem. Soc.* **2006**, *128*, 3526.
(8) Mostain, W. E.; Kepler, K.; Prakash, J. *J. Electrochim. Acta* **2007**, *52*, 2102.
(9) Lee, K.; Savadogo, O.; Ishihara, A.; Mitsushima, S.; Kamiya, N.; Ota, K.-I. *J. Electrochem. Soc.* **2006**, *153*, A20.
(10) Waits, R. K. *Thin film deposition and patterning*; Tompkins, H. G., Eds.; American Vacuum Society: New York, 1998.
(11) RaviPrakash, J.; McDaniel, A. H.; Horn, M.; Pilione, L.; Sunal, P.; Messier, R.; McGrath, R. T.; Schweighardt, F. K. *Sens. Actuators, B* **2007**, *120*, 439.
(12) Joshi, R. N.; Krishnan, S.; Yoshimura, M.; Kumar, A. *Nanoscale Res. Lett.* **2009**, *4*, 1191.
(13) Dagamseh, A. M. K.; Vet, B.; Tichelaar, F. D.; Sutta, P.; Zeman, M. *Thin Solid Films* **2008**, *516*, 7844.
(14) Huang, C.-M.; Cheng, K.-W.; Jhan, Y.-R.; Chung, T.-W. *Thin Solid Films* **2007**, *515*, 7935.
(15) Kang, S. H.; Lim, J.-W.; Kim, H. S.; Kim, J.-Y.; Chung, Y.-H.; Sung, Y.-E. *Chem. Mater.* **2009**, *21*, 2777.
(16) Gu, L.; Luo, N.; Miley, G. H. *J. Power Sources* **2007**, *173*, 77.
(17) Radev, I.; Slavcheva, E.; Budevski, E. *Int. J. Hydrogen Energy* **2007**, *32*, 872.
(18) Chang, C.-L.; Hang, T.-C.; Ho, W.-Y.; Hwang, J. J.; Wang, D.-Y. *Surf. Coat. Technol.* **2006**, *201*, 4442.
(19) Whitacre, J. F.; Valdez, T. I.; Narayanan, S. R. *Electrochim. Acta* **2008**, *53*, 3680.
(20) Jansen, J. A.; Wolke, J. G. C.; Swann, S.; Van Der Waerden, J. P. C. M.; De Groof, K. *Clin. Oral Implants Res.* **1993**, *4*, 28.
(21) Socol, G.; Macovei, A. M.; Miroiu, F.; Stefan, N.; Duta, L.; Dorcioman, G.; Mihailescua, I. N.; Petrescu, S. M.; Stan, G. E.; Marcov, D. A.; Chiriac, A.; Poeata, I. *Mater. Sci. Eng., B* **2010**, *169*, 159.
(22) Ma, Z. Q.; Cheng, P.; Zhao, T. S. *J. Membr. Sci.* **2003**, *215*, 327.
(23) Yoon, S. R.; Hwang, G. H.; Cho, W. I.; Oh, I.-H.; Hong, S.-A.; Ha, H. Y. *J. Power Sources* **2002**, *106*, 215.
(24) Wang, C. H.; Du, Y. Y.; Tsai, Y.-T.; Chen, C.-P.; Huang, C.-J.; Chen, L. C.; Chen, K. H.; Shih, H.-C. *J. Power Sources* **2007**, *171*, 55.
(25) Wan, C.-H.; Lin, M.-T.; Zhuang, Q.-H.; Lin, C.-H. *Surf. Coat. Technol.* **2006**, *201*, 214.
(26) O'Hayre, R.; Lee, S.-J.; Cha, S.-W.; Prinz, F. B. *J. Power Sources* **2002**, *109*, 483.
(27) Bhardwaj, N.; Kundu, S. C. *Biotechnol. Adv.* **2010**, *28*, 325.
(28) Huang, Z.-M.; Zhang, Y.-Z.; Kotaki, M.; Ramakrishna, S. *Compos. Sci. Technol.* **2003**, *63*, 2223.
(29) Dong, Z.; Kennedy, S. J.; Wu, Y. *J. Power Sources* **2011**, *196*, 4886.
(30) Shabani, I.; Hasani-Sadrabadi, M. M.; Haddadi-Asl, V.; Soleimani, M. *J. Membr. Sci.* **2011**, *368*, 233.
(31) Zhang, W. *ECS Interface* **2010**, *19*, 51.
(32) Otaño, W.; Otero, A. O.; Otaño, J. M.; Otaño, C. S.; Santiago, J. J.; Pantojas, V. M. *Mater. Res. Symp. Proc.* **2007**, *948*, 0948-B05-12.
(33) Arroyo-Ramírez, L.; Figueroa, Y.; Rodríguez, D.; Otaño, W.; Cabrera, C. R. *ECS Trans.* **2010**, *28*, 1.
(34) Pantojas, V. M.; Rodríguez, D.; Morell, G.; Rivera, A.; Ortiz, C.; Santiago-Avilés, J. J.; Otaño, W. *J. Nanophotonics* **2008**, *2*, 021925.
(35) Bard, A. J.; Faulkner, L. R. *Electrochemical Methods: Fundamentals and Applications*, 2nd ed.; Wiley: New York, 2001.
(36) She, P. L.; Yao, S. B.; Zhou, S. M. *Chin. Chem. Lett.* **1999**, *10*, 407.
(37) Grdén, M.; Lukaszewski, M.; Jerkiewicz, G.; Czerwinski, A. *Electrochim. Acta* **2008**, *53*, 7583.
(38) Fouda-Onana, F.; Bah, S.; Savadogo, O. *J. Electroanal. Chem.* **2009**, *636*, 1.
(39) Son, W. K.; Youk, J. H.; Lee, T. S.; Park, W. H. *Polymer* **2004**, *45*, 2959.